IEEE Access
Multidisciplinary | Rapid Review | Open Access Journal

Received 18 July 2023, accepted 3 September 2023, date of publication 8 September 2023, date of current version 13 September 2023.

Digital Object Identifier 10.1109/ACCESS.2023.3313200

RESEARCH ARTICLE

An Investigation on the Effects of Beam Squint Caused by an Analog Beamformed User Terminal Utilizing Antenna Arrays

RAED A. ABD-ALHAMEED[1], (Senior Member, IEEE), YIM FUN HU[1], (Senior Member, IEEE), YASIR AL-YASIR[1,2], (Member, IEEE), NASER OJAROUDI PARCHIN[3], (Senior Member, IEEE), AND ATTA ULLAH[1]

[1]Bradford-Renduchintala Centre for Space AI, Faculty of Engineering and Informatics, University of Bradford, BD7 1DP Bradford, U.K.
[2]Skyrora Ltd., G68 9LD Glasgow, U.K.
[3]School of Computing, Engineering and the Built Environment, Edinburgh Napier University, EH10 5DT Edinburgh, U.K.

Corresponding author: Raed A. Abd-Alhameed (r.a.a.abd@bradford.ac.uk)

This work was supported in part by the Satellite Network of Experts V under Contract 4000130962/20/NL/NL/FE, and in part by the Innovation Program under Grant H2020-MSCA-ITN-2016 SECRET-722424.

ABSTRACT In the equivalent frequency-based model, the antenna array gain is utilised to characterise the frequency response of the beam squint effect generated by the antenna array. This impact is considered for a wide range of uniform linear array (ULA) and uniform planar array (UPA) designs, including those with and without tapering configurations. For a closer look at how the frequency response of the array adapts to the variations in the incidence angle of the signal, the bandwidth of the spectrum is varied and investigated. To study this effect, we have considered using the gain array response as an equivalent channel model in our approach. Beam squinting caused by distortion in the frequency response gain can be verified by one of two equalisers: a zero-forcing (ZF) equaliser or a minimum mean square error (MMSE) equaliser. Different cases with their analysis and results are studied and compared in terms of coded and uncoded modulations.

INDEX TERMS Equaliser, minimal mean square error, uniform linear array, uniform planar array.

I. INTRODUCTION

The data rate at 4G LTE systems is limited to a certain level in wireless communications thereby the need to introduce the next generation 5G cellular communications that would provide a higher data rate compared to the current LTE spectrum [1]. The introduction of a new radio spectrum is required to achieve a higher data rate in cellular communications. A potential millimetre wave band could be used for 5G or multiple bands can be integrated and/or aggregated [2]. However, the millimetre wave signal is significantly affected by a high path loss which is typically assumed to be 20 dB or more [3].

This kind of attenuation can be offset, rectified, or compensated by using many or a large number of antennas with phased-array beamforming technology. These array structures result from fewer wavelengths and can be deployed in several mobile applications [4]. Ideally, a phase shifter in the phased array should have the same phase shift for the given frequencies within the spectrum band of considerations [5], [6], [7].

Whenever the signal bandwidth is very small, a time delay will be relatively approximate to a phase shift. However, if the broadside is far away from the angle of arrival (AOA) or angle of departure (AOD) for a signal with a larger bandwidth, phase shifters may have different time delays for different frequencies, and the narrowband approximation degrades and/or breakdown. This will result in the array response varying over frequencies and their beams other than the carrier ''squint'', as a function of frequency [6], and it is called beam squint [7]. For either AOA or AOD, beam squint clearly introduces array gain and phase variations over frequency [8], as well as reducing channel capacity [9]. The number of antennas in the array as well as the bandwidth can increase the effect of beam squint [8].

The beam squint, also known as a variation in steering angle against frequency, is brought on by a phase shift that

The associate editor coordinating the review of this manuscript and approving it for publication was Zaharias D. Zaharis.

is approximately equivalent to a time delay. This issue is not present when beam steering is implemented using units that display a true-time delay [10]. The spatial wideband effect [11], [12] is what happens when you combine a high bandwidth with a large number of antennas. This generates a non-negligible propagation delay across the aperture of the antenna array in time-domain sample periods, which in turn, induces beam squint in the frequency domain [13]. Many research studies have been conducted to reduce and/or eliminate beam squint, including true time delay [14]. On the other hand, significant insertion loss, excessive power consumption, high implementation cost, and large hardware size in such approaches are not applicable to mobile wireless communications [8], [14]. True-time delay may be included in the digital signal processor (DSP) logic as well as the digital beamforming algorithms when using digital beamforming. Because of this, a phased array design, in which every element is digitalized, would lend itself readily to overcoming the beam squint issue, while giving the greatest amount of programmable flexibility simultaneously [10].

The power requirements, physical dimensions and cost of such systems may all be problematic. To offset and/or compensate for a higher path loss and to achieve higher directional gain, beamforming is employed in millimetre wave bands [4], [16]. However, the short wavelength of a millimetre wave allows the integration of a large number of antennas into a small phased array, which is applicable in mobile devices. There are three modes of arrangement for millimetre wave beamforming, which include analogue, hybrid, and digital beamforming. The following solutions to this problem can be proposed:

- Analogue beamforming is supported by Equalizer to fix the frequency dependency of the array gain.
- In addition to the point made above, we will test various coding techniques to improve the bit error rate (BER) caused by the squint effects. These are different solutions that can be considered for this problem.

These, in our opinion, have the potential to give some natural beam squint reduction that should be taken into consideration. Beam squint is only subject to the subarray, which has a much wider beamwidth, so it is more tolerant to a beam angle deviation within the analogue beamforming. This effect can partially be reduced when hybrid beamforming architecture is implemented with phase shifters in the subarrays followed by true time delay in the digital beamforming [10]. Beam squint is defined as a deviation in steering angle versus frequency and is caused by an approximate frequency-dependent phase steering angle of the incident beam on the array. This issue is not present when true-time delay units are used for the implementation of beam steering. In this study, we strongly aimed to keep costs low, and one way we achieve this is by considering analogue beamforming techniques that just include phase shifters.

In most cases, this boils down to the ease of design and availability of integrated circuits for phase shifters versus time delays. Transmission lines of some examples are used to implement time delays, and the aperture size plays a role in determining the overall amount of delay that is required. However, there are families of true-time delay integrated

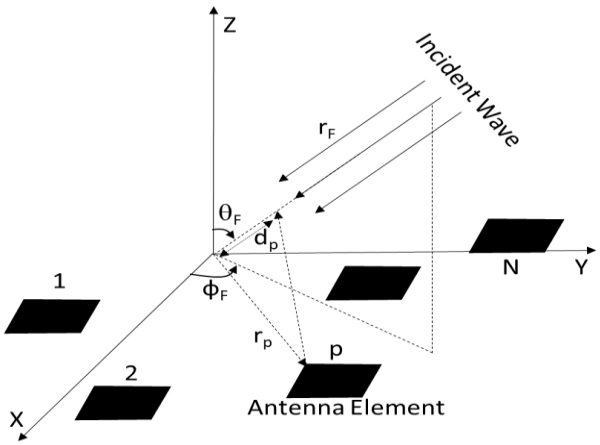

FIGURE 1. The geometry of the antenna array.

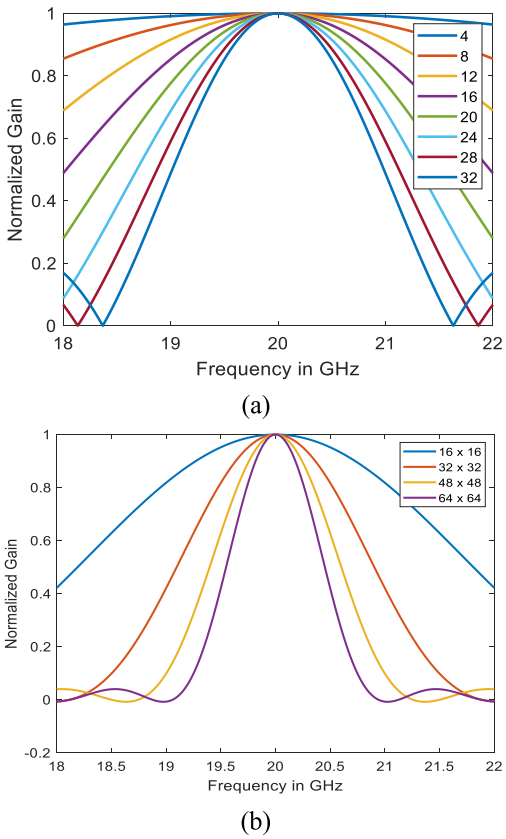

FIGURE 2. The normalised frequency gain response for various numbers of elements, and incident angles $\theta = 60°$ and $\phi = 50°$ (a) ULA and (b) UPA.

circuits (ICs) that are under development, and they may become much more popular for phased array implementations [10], [11], [12], [13]. To this day, the majority of the analogue beamforming ICs that are now available are based on phase shift. Analogue beamforming with phased arrays is an interesting and promising technique for 5G wireless communications in millimetre wave spectrums. However, beam squint offsets degrade the output performance of analogue beamforming for wide-band systems with numerous

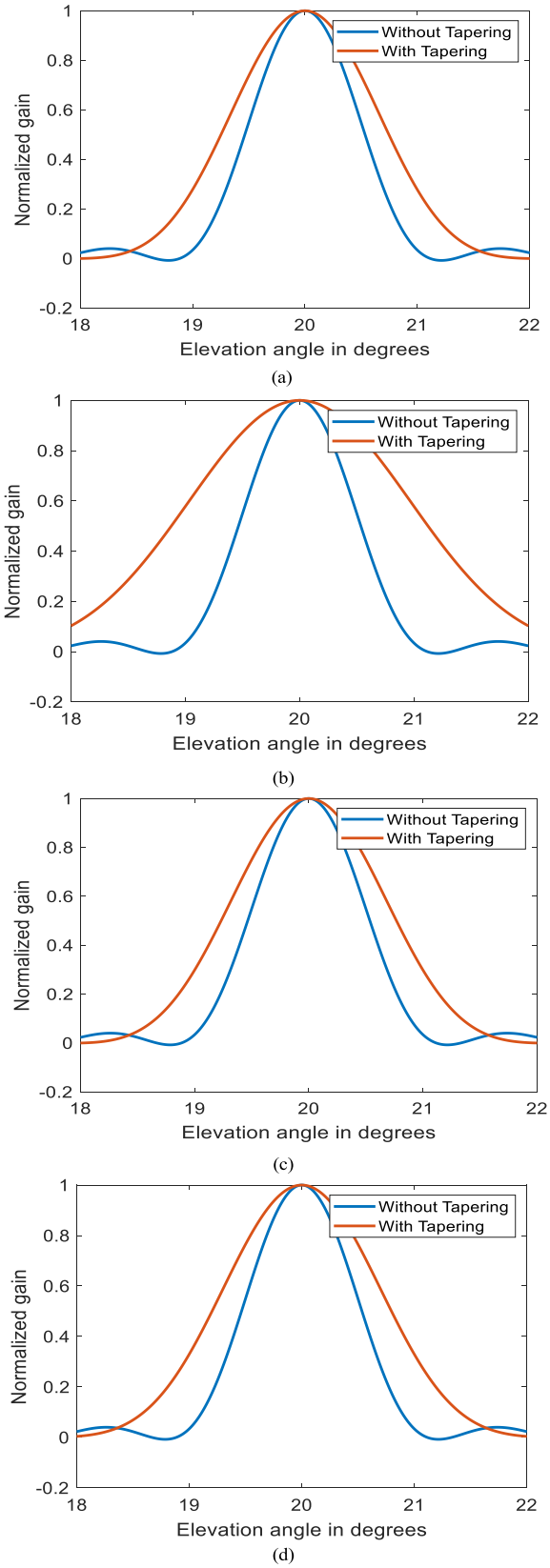

FIGURE 3. Frequency gain response with and without tapering for UPA 54 × 54; a) Taylor, b) Chebyshev, c) Kaiser and d) Hamming.

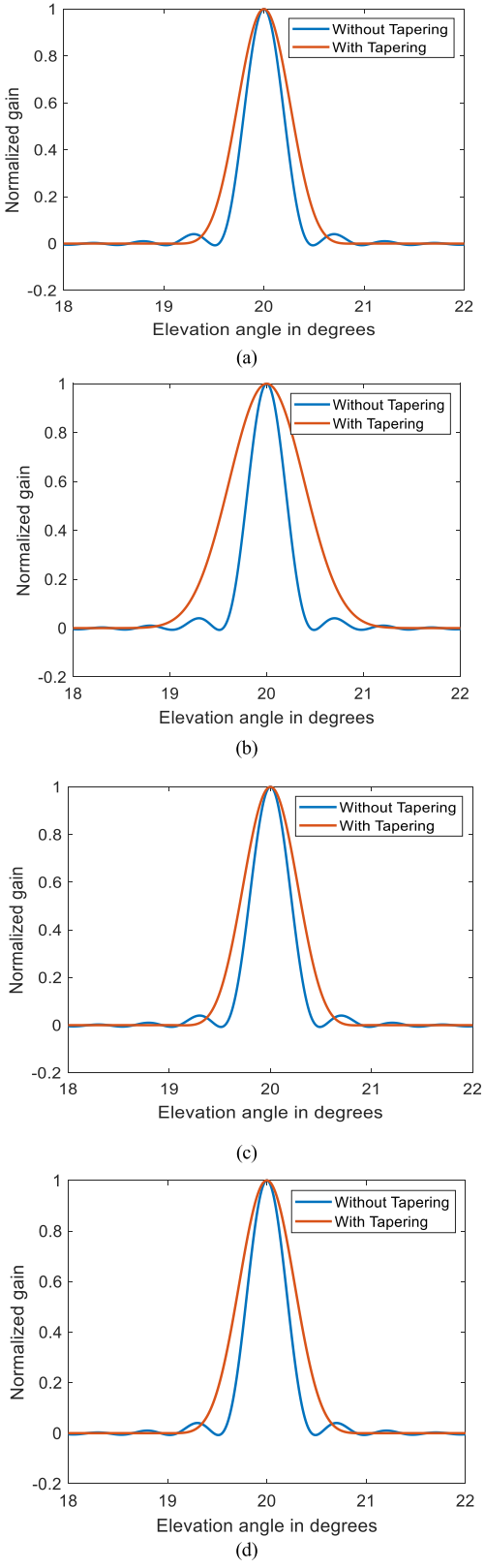

FIGURE 4. Frequency gain response with and without tapering for UPA 134 × 134; a) Taylor, b) Chebyshev, c) Kaiser and d) Hamming.

antennas. This is because the array output, power compensation, and channel response vary with frequencies [17].

In this study, we considered the impacts of the beam squint as a function of the incidence angles by integrating the array

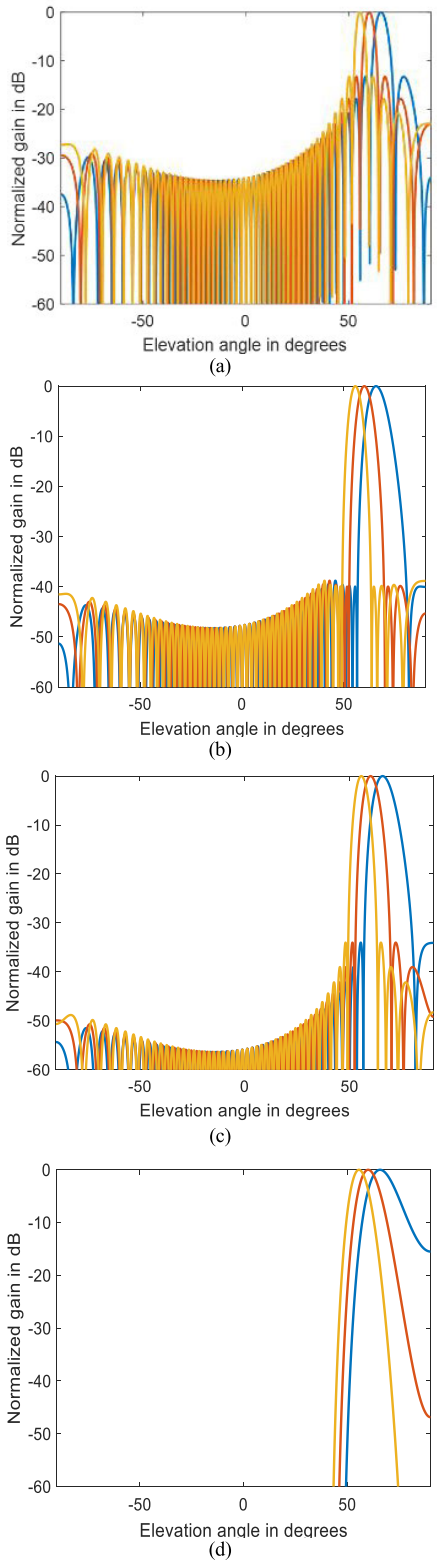

FIGURE 5. The normalised radiation patterns for 54 ULA for a circular polarization antenna array; a) without tapering, b) with Taylor tapering, c) with Kaiser tapering, d) with Chebyshev tapering; the elevation angle is 60° and max bandwidth is 2 GHz.

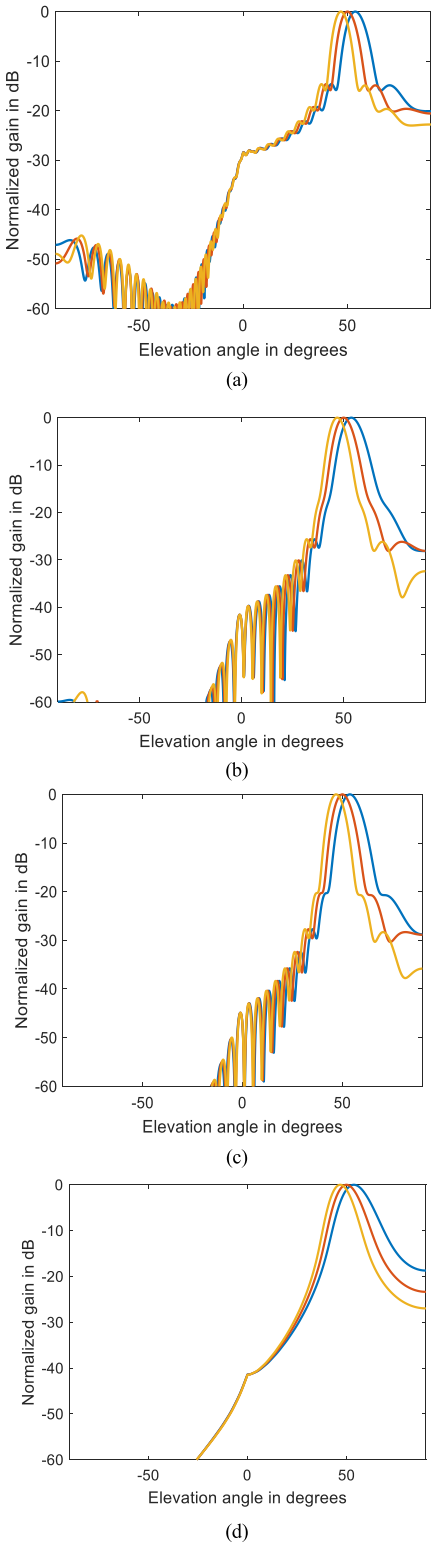

FIGURE 6. The normalised radiation patterns for 54 × 54 UPA with circular polarization antenna array; a) without tapering, b) with Hamming tapering, c) with Kaiser tapering, d) with Chebyshev tapering; the elevation angle is 50° and max bandwidth is 2 GHz.

gain as a frequency-dependent function. We have established general equations (2D and 3D) for the inclusion of the tapering and radiation pattern for each antenna element in the array response. These equations were derived based on the arbitrary array geometry. After this step, the gain is included inside a communication model that suits the functioning of a

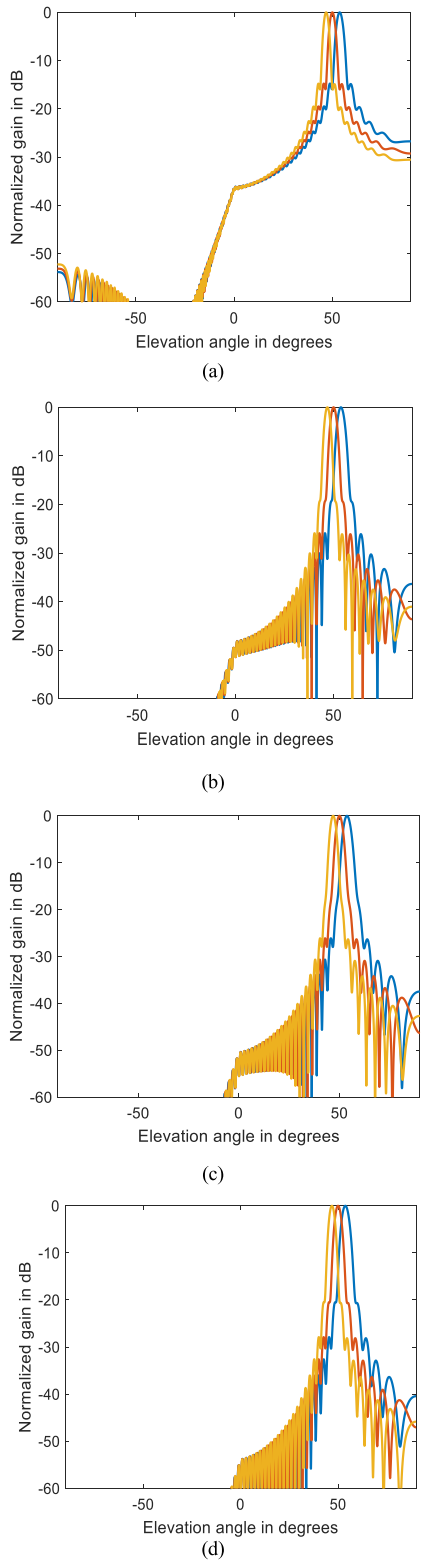

FIGURE 7. The normalised radiation patterns for 134 × 134 UPA of a circular polarization antenna array; a) without tapering, b) with Taylor tapering, c) with Hamming tapering, d) with Kaiser tapering; the elevation angle is 50° and max bandwidth is 2 GHz.

SIMO system in which the gain was added as either frequency response or impulse response to represent an equivalent channel model. Ultimately, this model was applied to improve the operational performance of the SIMO systems. After that, the model of the system comprises an encoding technique in addition to a range of modulations, matching filters, and Gaussian noise. In addition to this, we proposed the use of equalisers as a method of overcoming the amplitude distortion that was caused by the array gain response. This was investigated to address the issue of such effects. In addition, we have also shown a comprehensive study of the impact of squinting on BER for M-QAM, M-APSK, and DVB-S2X.

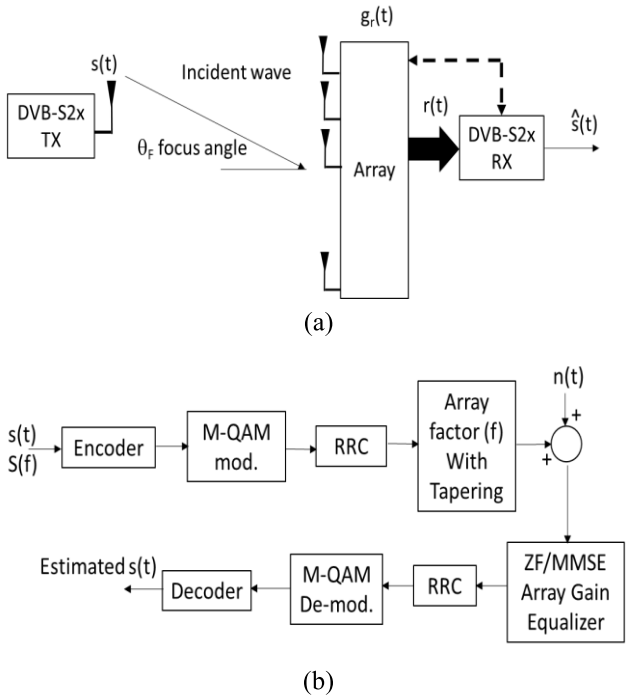

FIGURE 8. (a) Description of the proposed channel and squinting effect for DVB-S2x model, (b) The simulated model.

II. THE RESPONSE FUNCTION OF THE ARRAY GAIN WITH TAPERING

We can assume that have a number of elements to reform a planer antenna array similar to the one shown in Figure 1. To consider a reference at the origin, one can predict the delay distance between the incident wave and the vector position of the antenna element using the dot product between the two vectors as follows:

$$d_p = \mathbf{r}_i \bullet \mathbf{r}_p \tag{1}$$

where r_i and r_p are the incident wave vector and the pth vector from a reference point to the centre of a pth antenna element at the array. These are given by:

$$\mathbf{r}_i = \cos(\phi_i)\cos(\theta_i)\widehat{a}_x + \sin(\phi_i)\cos(\theta_i)\widehat{a}_y - \sin(\theta_i)\widehat{a}_z$$
$$\mathbf{r}_p = x_p\widehat{a}_x + y_p\widehat{a}_y + z_p\widehat{a}_z$$

And ϕ_i and θ_i are the azimuth and elevation angles of the incident angle or sometimes called the focus angles ϕ_F and θ_F.

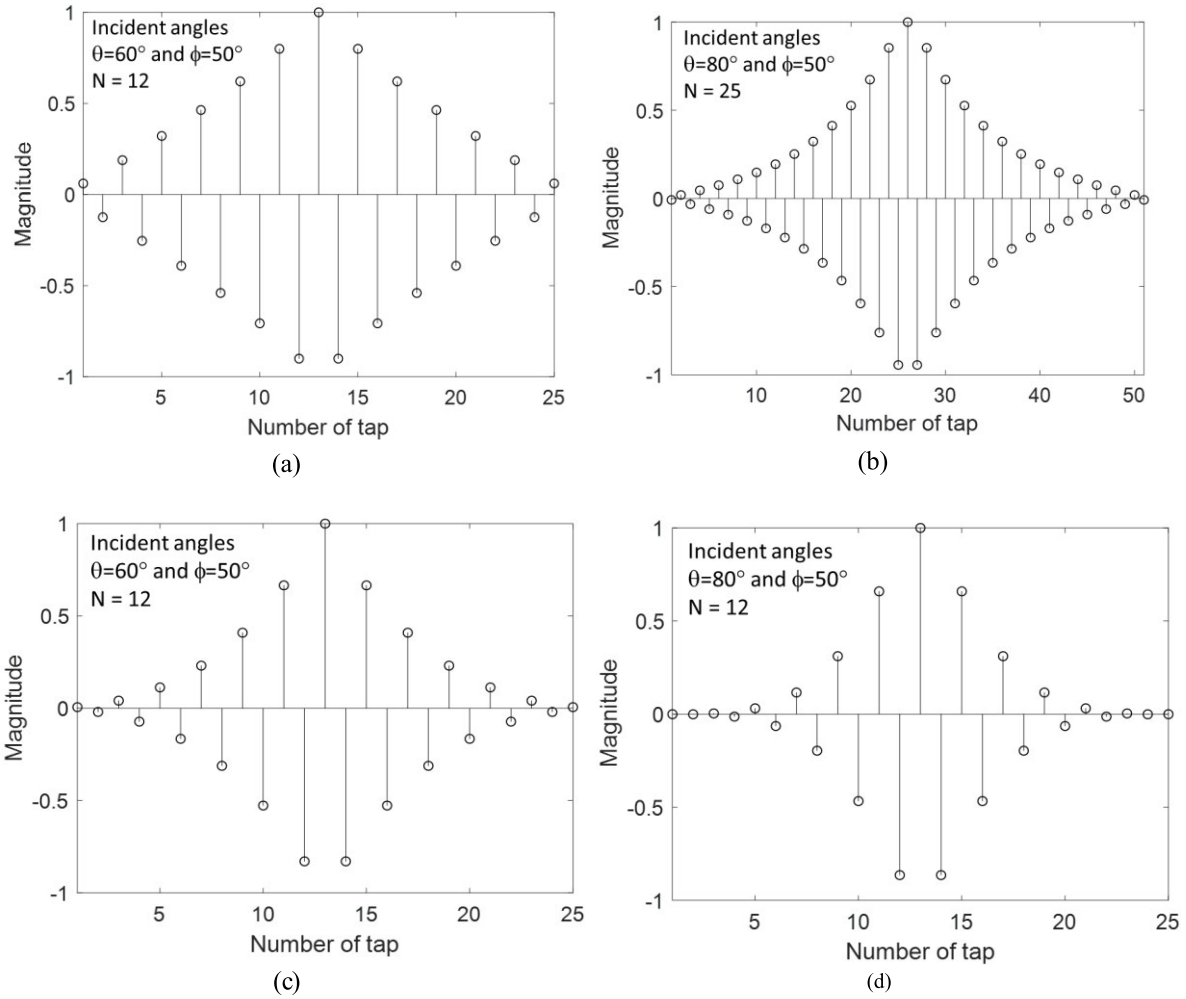

FIGURE 9. The tap coefficients for ZF and MMSE equalizers of 54 × 54 UPA; a) and b) ZF without and with tapering respectively, c) and d) MMSE without and with tapering respectively, with a noise variance of 0.05.

Where r_i and r_p are the incident wave vector and the vector from a reference point to the centre of each antenna element at the array, these are given by:

Now, the phase delay for pth antenna element can be given by:

$$P_{dp} = e^{-jk(\mathbf{r}_i \bullet \mathbf{r}_p)} \tag{2}$$

Eq. 2 is a general case that could include 2D or 3D location antenna array geometries. Now considering the tapering coefficients all over the antenna elements, the array gain response, when the steering angle is set equal to the focus angle (i.e., $\theta_s = \theta_F = \theta$, $\phi_s = \phi_F = \phi$; θ_s and ϕ_s are the steering angles in elevation and azimuth respectively; θ_F and ϕ_F are the focus angles in elevation and azimuth), including the effects of the antenna radiation fields, can be represented as follows.

$$G(\theta, \phi, f) = \sum_{p=1}^{N} c_p f_p(\theta, \phi) e^{-j2\pi(\mathbf{r}_i \bullet \mathbf{r}_p)\frac{f_c}{c}(\frac{f}{f_c}-1)} \tag{3}$$

where f_c is the centre frequency, c_p is the pth tapering coefficient of the tapering applied to each antenna element. f_p is the field strength in the direction of θ, and ϕ. c is the speed of light. And N is the number of antenna array elements.

The array gain for a simplified geometry of ULA and UPA, considering the reference phase at the centre of the arrays and assuming the steering angle (or focus angle) is equal to the incident angle without embedding the tapering coefficients and the elements radiation Eq. 3 will be reduced to the following expression:

ULA array gain:

$$G_r(\phi_i, f) = \frac{\sin(\frac{N_x\pi}{2}(\sin(\phi_i)(\frac{f}{f_c}-1))}{\sqrt{N}\sin(\frac{\pi}{2}\sin(\phi_i)(\frac{f}{f_c}-1))} \tag{4}$$

UPA array gain:

$$G_r(\theta_i, \phi_i, f) = \frac{\sin(\frac{N_x\pi}{2}\sin(\theta_i)\cos(\phi_i)(\frac{f}{f_c}-1)}{\sqrt{N_x}\sin(\frac{\pi}{2}\sin(\theta_i)\cos(\phi_i)(\frac{f}{f_c}-1)} \times \frac{\sin(\frac{N_y\pi}{2}\sin(\theta_i)\sin(\phi_i)(\frac{f}{f_c}-1)}{\sqrt{N_y}\sin(\frac{\pi}{2}\sin(\theta_i)\sin(\phi_i)(\frac{f}{f_c}-1)} \tag{5}$$

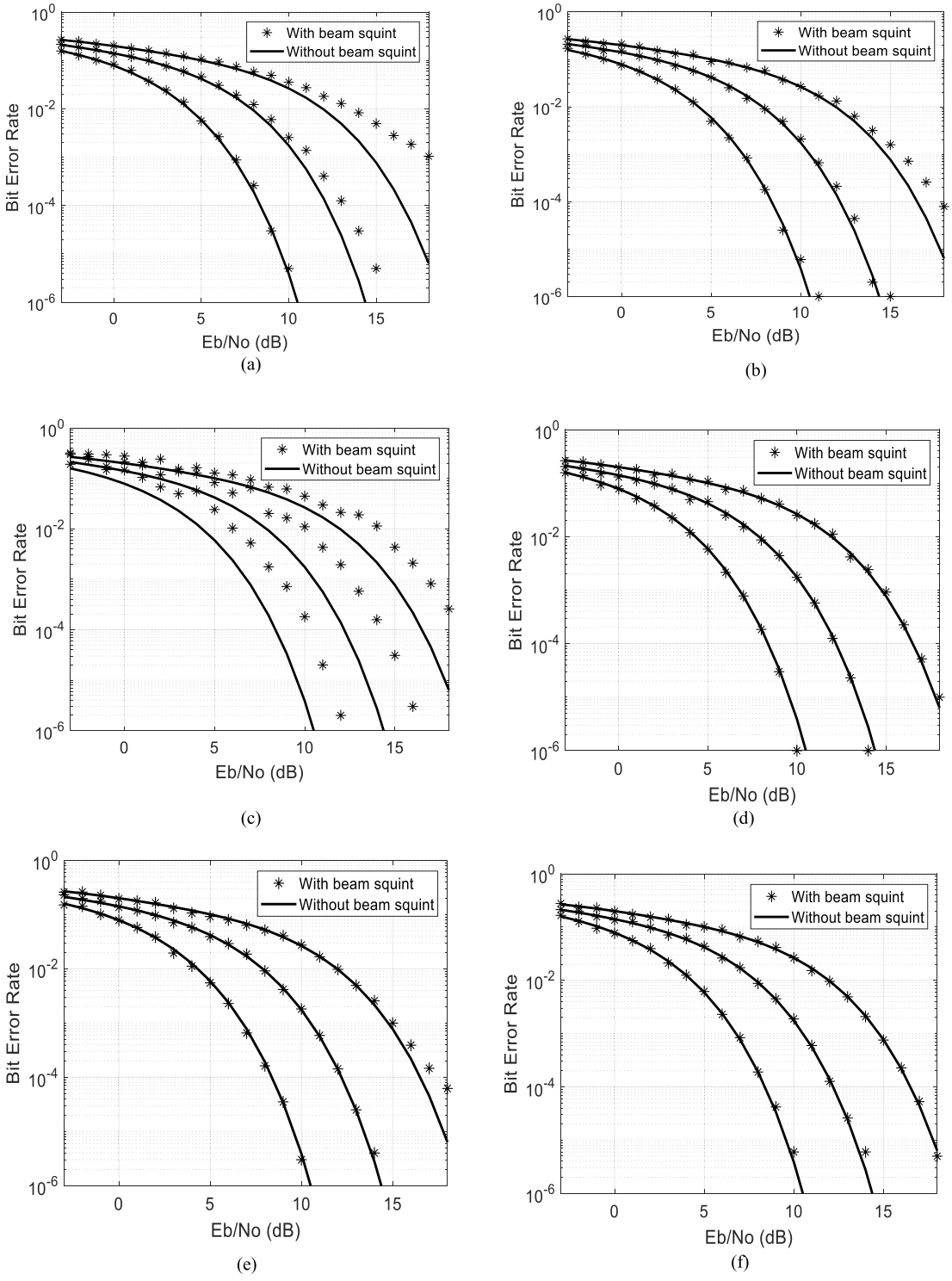

FIGURE 10. The variations of the BER for 4, 16 and 64 QAM modulation for 54 × 54 UPA; a) without tapering and equalizer, b) with tapering only, c) with ZF equalizer only, d) with tapering and ZF equalizer, e) with MMSE equalizer only, f) with tapering and MMSE equalizer.

where $\phi_s = \phi_i$ and $\theta_s = \theta_i$. N_x is the number of ULA elements along the x-axis. N_x and N_y are the dimensions of the array elements in the x and y axes, respectively.

Based on Eqs 4 and 5, the variations of the frequency gain responses for incident angles $\theta = 60°$ and $\phi = 50°$ on ULA and UPA over various numbers of elements, excluding

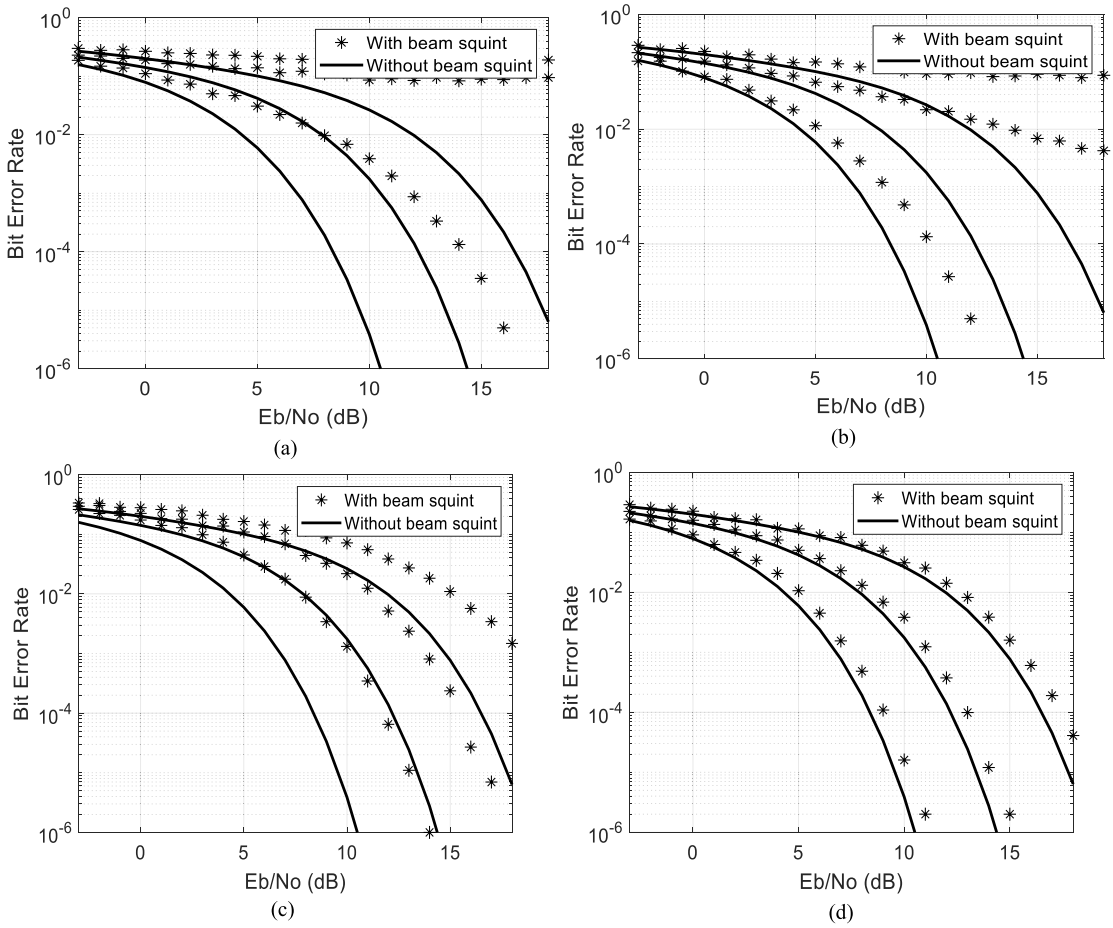

FIGURE 11. The variations of the BER for 4, 16 and 64 QAM modulation for 134 × 134 UPA; a) without tapering and equalizer, b) with tapering only, c) with equalizer, d) with tapering and equalizer; Similar Square root raised cosine FIR filter as in Figure 9.

tapering and radiation pattern of antenna elements, are shown in Figure 2. It is very clear to see the effects of the beam squint as an equivalent to the frequency-selective channel using analogue beamforming.

For the gain response shown in Eq. 3, we have studied four types of tapering over uniform planer array antenna. These are: a) Taylor (with 4 constant sidelobes level adjacent to the main lobe at −40 dB), b) Hamming (apply hamming window function), c) Kaiser (with $\beta = 4.5$ as Kaiser window parameter that affects the sidelobes attenuation), and d) Chebyshev (apply Chebyshev window function). We have applied this over a circularly polarized antenna array. The tapering coefficient elements over various array sizes operated at centre frequency 20 GHz have been demonstrated based on the variations of the BER for various modulations.

The computed gain response with and without tapering is presented in Figures 3 and 4, based on the above-suggested coefficients. The variations of the gain response were computed over 4GHz bandwidth and a centre frequency of 20 GHz, based on the elevation angle 60° and azimuth 50°. From the set of the results for 54 × 54 and 134 × 134 UPAs (this is equivalent to 40 × 40 cm^2 and 1m x 1m apertures respectively), the tapering has improved the response to avoid the nulls caused by the wide bandwidth. It also smoothes the response compared to the case without the tapering process. The variations of the gain response by applying Taylor, Kaiser and Hamming tapering are quite similar for both UPAs; whereas, Chebyshev tapering is proved to be consistent with the case of without tapering with small elevation angles. Nevertheless, this tapering will affect the variations of the beamwidth compared to the other three tapers and thus might cause another type of interference from the wider beamwidth generated. The following results are some examples of beam squinting with and without tapering that clearly show the main contribution of the tapering to the operation of the antenna array.

III. BEAM SQUINTS WITH AND WITHOUT TAPERING

The normalized radiation patterns with and without tapering, including beam squint effects, are shown in Figures 5, 6 and 7. In these examples, we have tried to achieve minimum sidelobe levels at higher elevation angles for the four tapering methods applied over ULA and UPA array antennas. The colours of the given plots are blue at fc-BW/2, red at fc, and orange at fc+BW/2 (BW is the spectrum Bandwidth). Obviously, the results from this will be utilised to compute the BER rate in the next sections. The sizes of the UPAs are similar to the ones given in the previous section.

From Figure 5, it can be observed that the tapering for 54 ULA provides good radiation performance with low sidelobes levels for all the tapering applied. Due to the widening window of the Chebyshev, this distorts the beam at a higher angle. It was verified that this type of tapering could be useful with an array operating at an elevation angle of less than ±60°. The tapering with Taylor and Kaiser is quite similar except that Kaiser tapering has lower sidelobes levels away from the main lobe. Hamming tapering is not presented here since its performance is quite similar to Taylor tapering.

Figures 6 and 7 show the variations of the radiation patterns for 54 × 54 and 134 × 134 UPAs, respectively based on circular polarized antennas. Again, the maximum bandwidth considered for both is 2 GHz. The focus angle is 50° elevation and 0° azimuth. It is easy to notice the low sidelobe levels for all tapering applied compared to the case without tapering. The variations over the three tapering coefficients are comparable to each other. It can also be indicated that the Chebyshev widens the width of the main lobe compared to other tapering applied. It should be noted that the sidelobe levels are between 24 to 28 dB with tapering compared to 13 dBs without such a wide scanning angle for both ULAs and UPAs.

Figures 6 and 7 show a very clear message on how wider beam squint could be when a higher steering angle near 90 degrees is required, however, the tapering enhanced the reliability to widen the gain response and avoid the nulls near the edges of the wide bandwidth. It can also be concluded that the array performance could be a trade-off by the operating bandwidth at higher steering angles.

IV. PROPOSED SYSTEM MODEL AND SIMULATED RESULTS

We have assumed the array gain response as the channel model of the whole system model to make sure that we are able to take into account the beam squint effects only, as shown in Figure 8a. Figure 8b shows the block diagram of the proposed model with the gain response channel equalizer and array antenna tapering that has been considered in this work.

Since we have applied analogue beamforming, thus the received signal model with array gain response (i.e. the results of the kroneker product of the incident wave with conjugate steering vector) is excluding the channel effects and is taking into account the array gain only with AWGN, leading to the following:

$$r_x(t) = g_r(t) * s(t) + n(t) \tag{6}$$

$$R_x(f) = G_r(f).S(f) + N(f) \tag{7}$$

where $g_r(t)$ and $G_r(f)$ are the receiver array gain in the time and frequency domains, respectively. It should be noted that these equations are excluding tapering and antenna patterns. Gr(f) is given by Eqns 5 and 6 for ULA and UPA configurations, respectively. s(t) and S(f) are the transmitted modulated signal in the time and frequency domains respectively. $r_x(t)$ and $R_x(f)$ are the received signal in the time and frequency domains, respectively. n(t) and N(f) are the AWGN in time and frequency domains, respectively.

Two equalizers are deployed to compensate for the distortion caused by the array gain response. These are ZF and MMSE with 2N+1 number of taps. In ZF equalization, the tap coefficients of the ZF equalizer can be estimated and determined by solving $2N_s + 1$ linear equations, simply by

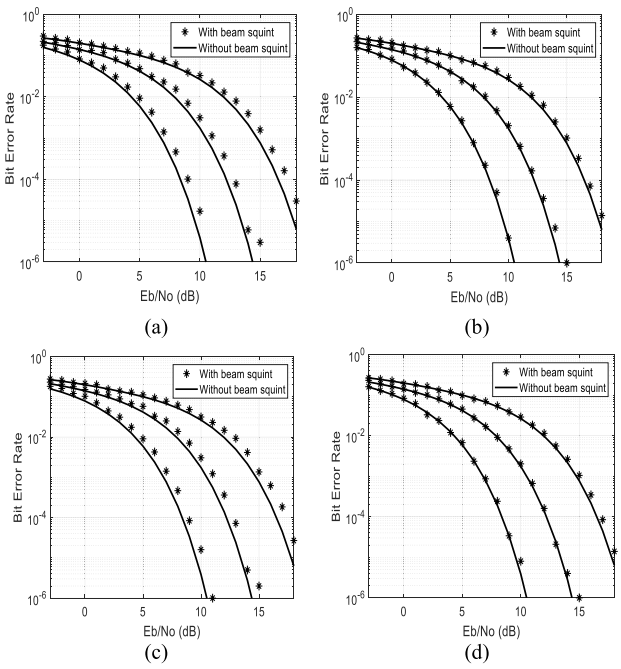

FIGURE 12. The variations of BER for various M-QAM modulations; a) ZF-Frequency domain, b) MMSE-Frequency domain, c) ZF-Time domain, b) MMSE-Time domain.

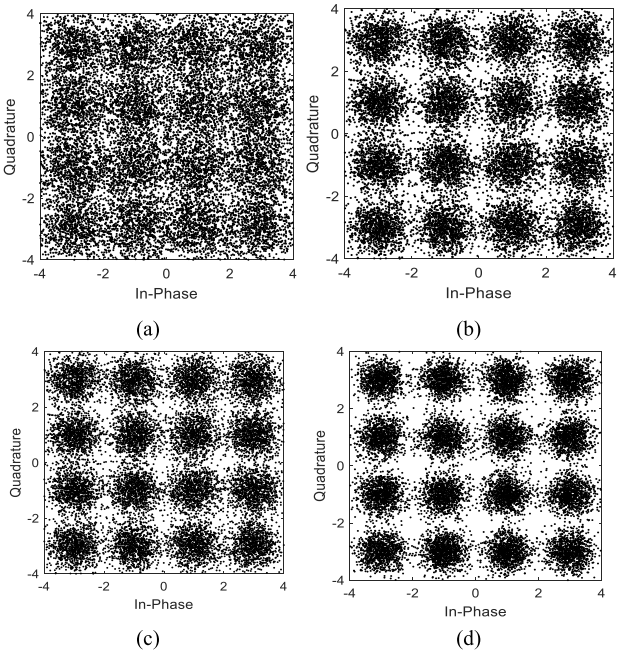

FIGURE 13. Scatterer plot for 16-QAM of 134 × 134 UPA array; a) without tapering and equalizer, b) with tapering only, c) with equalizer only, d) with tapering and equalizer. (All other parameters are the same as the previous example).

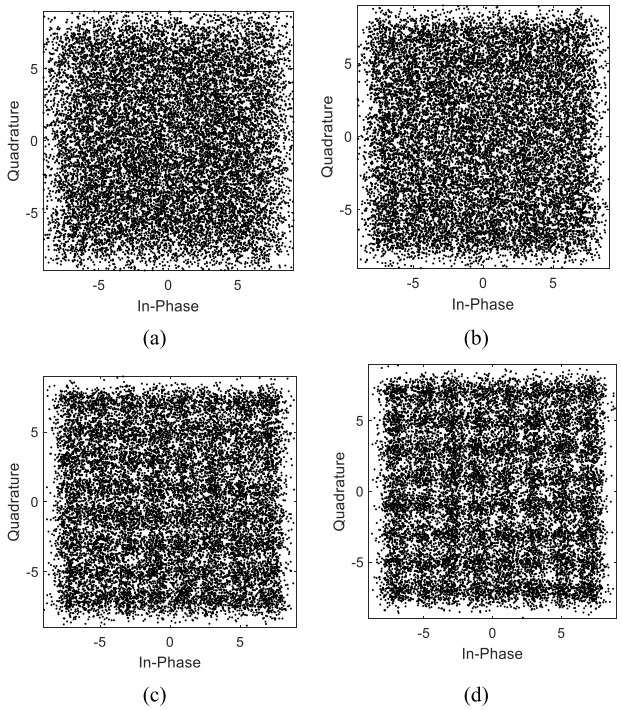

FIGURE 14. Scatterer plot for 16-QAM of 134 × 134 UPA array; a) without tapering and equalizer, b) with tapering only, c) with equalizer only, d) with tapering and equalizer. (All other parameters are the same as the previous example).

applying the following:

$$\sum_{n=-N_s}^{N_s} c_n g(m-n) = \begin{cases} 1, & m=0 \\ 0, & m=\pm1, \pm2, \ldots, \pm N_s \end{cases} \quad (8)$$

where $g(t)$ is the impulse response of the gain response with causal ISI of length L, c_n represents the *nth* coefficient of the $2N_s + 1$ equalizer tap coefficients, and N_s is the frequency sampling which is generally chosen sufficiently large so that the equalizer spans the length of the ISI.

ZF equalizer could lead to a degraded operation outcome due to noise enhancement as we will show some results later. The significant noise enhancement is due to the fact when the channel response is small, the channel equalizer compensates by placing a large gain in that frequency range, thus enhancing noise in that frequency range; whereas the MMSE equalizer selects the channel equalizer taps such that the combined power in the residual ISI and the additive noise at the output of the equalizer are minimized. This equalizer is more robust than a ZF equalizer in the presence of a large ISI. It minimizes the mean-square error of all the ISI terms plus noise. In MMSE equalization for a channel with the causal ISI of length L, the tap coefficients of the equalizer can be determined by solving the $2N_s + 1$ linear equations as follows

$$\sum_{n=-N_s}^{N_s} c_n \left(\sum_{k=0}^{L} g(k)g(k+m-n) + \sigma^2 \delta_{n-m} \right) = g(-m)$$
$$For\ m = -N_s, -N_s+1, \ldots\ldots\ldots N_s \quad (9)$$

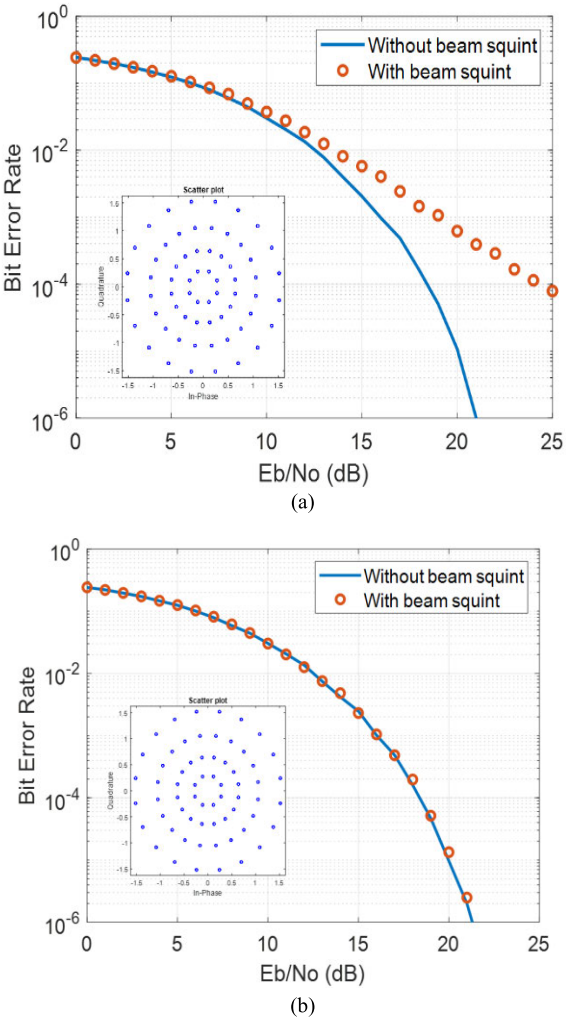

FIGURE 15. The variations of BER versus EbNo for 54 × 54 UPA applying 64-APSK over 2 GHz signal spectrum bandwidth and with similar square root raised cosine FIR filter used in Figure 8.

where δ_{n-m} is the Kronecker delta and σ^2 is the noise variance. It is important to note that the conditions for the optimum tap gains for MMSE equalizers are similar to those for ZF equalizers, except the autocorrelation function samples are used instead of the samples of the received pulse.

Different examples have been considered using Matlab codes with different array sizes for ULA and UPA configurations. In which, the frequency-dependent array gain is included. The source codes also introduce the tapering and the two-channel equalizers ZF and MMSE in Eqns 6 and 7 respectively. The bandwidth is also varied for many array sizes with and without tapering and channel equalizers.

Figure 9 shows the distributions of the coefficient taps for ZF and MMSE equalizers for two examples with and without tapering and two incident angles for 54 × 54 UPA. For the ZF equalizer example, Figures 9a and 9b show the coefficients without tapering and with tapering for incident angles of 60° and elevation angle of 80°, respectively. The azimuth angle is set at 50° for all sub-figures of Figure 9. N is set to 12 and 25 for Figures 9a and 9b, respectively. Figures 9c and 9d are

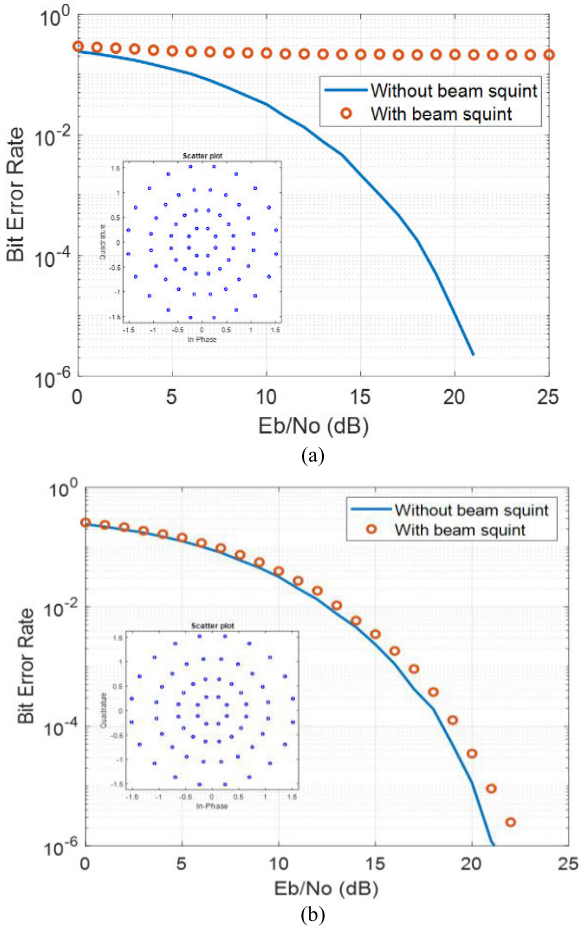

FIGURE 16. Figure 16. The variations of BER versus EbNo for 134 × 134 UPA applying 64-APSK over 2 GHz signal spectrum bandwidth and with similar square root raised cosine FIR filter used in Figure 9.

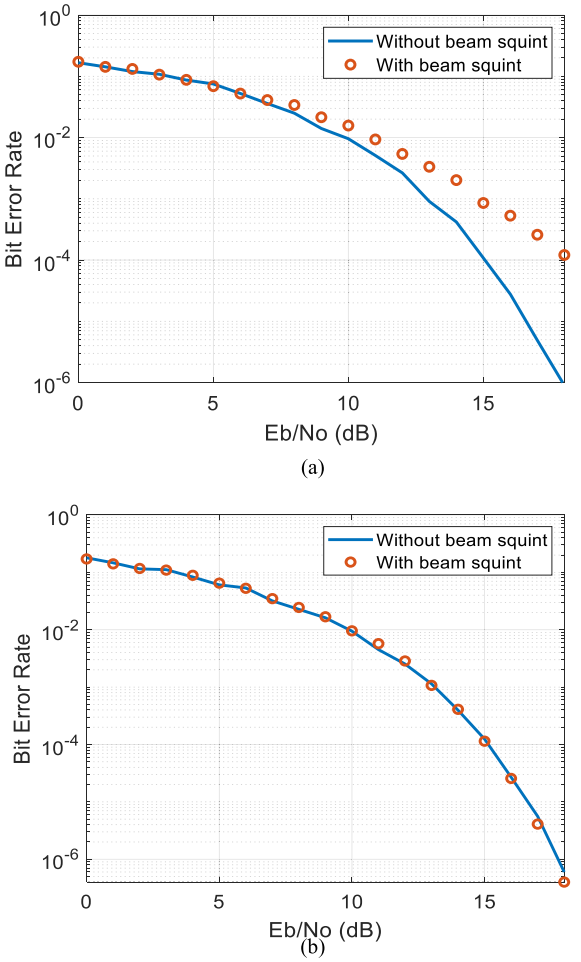

FIGURE 17. The variations of the BER for 32-APSK DVB-S2X, for an incident, angles 80°-elevation and 50°-azimuth; signal bandwidth is 2 GHz; a) without the tapering and equalizer, b) with Taylor tapering and MMSE equalizer.

the coefficients for the same UPA array used in ZF except for the variance of the noise which is set at 0.05 and N is kept at 12. The variations of tap coefficients are different between ZF and MMSE where the correlation and noise variance are applied at the MMSE equalizer only.

V. BER FOR UNCODED M-QAM WITH BEAM SQUINT

Figure 10 depicts the relationship between the BER and EbNo for three different uncoded M-order QAM modulations at $\theta = 80°, \phi = 0°$ of the UPA 54 × 54 array element. The bandwidth is 2 GHz and hamming tapering is applied. The model has applied square root raised cosine FIR filter with, roll-off = 0.25, Span symbols = 8 and Sample per Symbol = 4. ZF and MMSE equalizers are used to investigate the performance with beam squinting. The model also includes a square root raised cosine FIR filter (details are given within the title of the figure). The frame length is 16400. It is clear that better BER performance is achieved for the lower modulation. The BER obtained with tapering and equalizer matched the BER variation without squint effects. It is also noticed that by using an equalizer only, the MMSE outperforms the ZF equalizer. It also observed that the tapering could improve the BER at higher level modulation but less than the one achieved by the equalizer only. Various examples have been considered using Matlab codes with different array configurations, in which, the frequency-dependent array gain is included.

Figure 11 illustrates the variations of the BER with and without tapering and equalizer for the array size of 134 × 134 UPA. 4, 16 and 64 QAM level modulation is applied. The elevation and azimuth angles are 80° and 50° respectively. Taylor tapering coefficients are applied to this UPA array element. The bandwidth considered in this example was 2 GHz, in which, the impulse response of the array gain was applied in the time domain. The length of the frame size used is 16400. It is clear that the combination of tapering and MMSE equalizer is providing the optimum solution to resolve the effects of beam squinting in such a narrow beam for a wider aperture antenna array. It is also noted that the operation of the equalizer alone is better than tapering only.

A comparison between ZF and MMSE with tapering is demonstrated in Figure 12. The assumption applied in the previous example used here except the bandwidth was changed to 1.4 GHz. The solution was performed over both the time domain and frequency domain of the gain response. The figure illustrates that the MMSE outperforms the ZF.

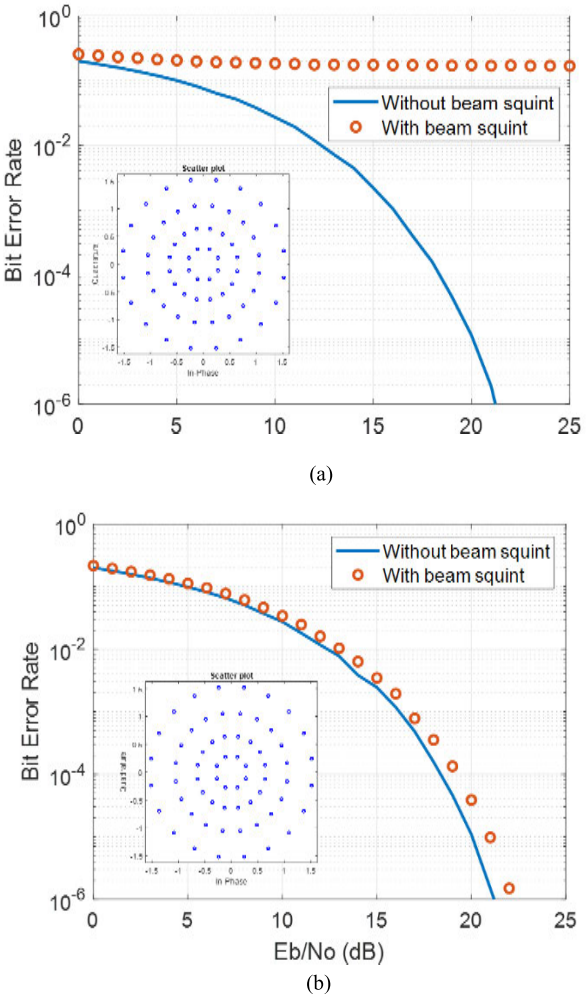

FIGURE 18. The variations of the BER for 64-APSK DVB-S2X, for an incident, angles 80°-elevation and 50°-azimuth; signal bandwidth is 2 GHz; a) without the tapering and equalizer, b) with Taylor tapering and MMSE equalizer.

Figures 13 and 14 show the variations of the constellation diagrams with beam squint of the previous example at Eb/No = 10dB only for 16 and 64 QAM modulations, respectively. These figures show the effects of beam squint which has a direct influence on the random distribution of the vector's consultation and how the combination of both tapering and the equalizer improves that process. It is observed that the equalizer has much more impact than the tapering alone, especially for high-level modulation.

A. BER FOR UNCODED 64-APSK WITH BEAM SQUINT

Figures 15 and 16 depict the relationship between the BER and EbN0 for two array sizes. The array sizes are 54 × 54 and 134 × 134 UPAs, respectively. The modulation applied is 64-APSK with a short frame length of 16400. The radius vector of the signal positions for this modulation is "radii = [0.19233 0.42307 0.692351 0.999998]". The incident angle for 54 × 54 and 134 × 134 UPAs are 60° and 80° respectively. For comparisons, we have included

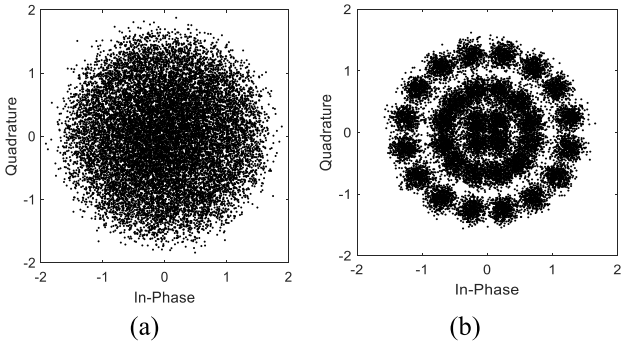

FIGURE 19. Scattering plot for 32-APSK, for Figure 15 at EbNo = 10dB; a) without tapering and equalizer, b) with tapering and equalizer.

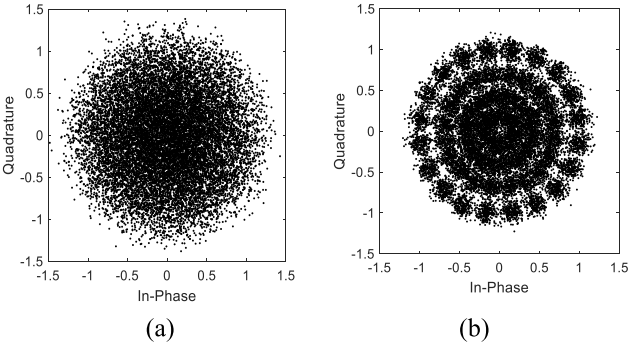

FIGURE 20. Scattering plot for 64-APSK, for Figure 16 at EbNo = 10dB; a) without tapering and equalizer, b) with tapering and equalizer.

no squint beam by considering an incident signal at 0° (Figures 15a and 16b). For this example and the following sections, the MMSE was applied with Taylor tapering. The model also includes a square root raised cosine FIR filter (details given within the title of the figure). It is observed that the inclusion of tapering and equalizer provides the required BER for the two elevation angles considered in both UPAs (Figures 15b and 16b). Also, for a lower elevation angle, the compensation of the beam squint is effective.

B. BER FOR CODED DVB-S2X WITH BEAM SQUINT

Figures 17 and 18 illustrate the case study for the DVB-S2X system evaluation with the 32-APSK and 64-APSK coded constellations including the beam squint effect and with and without the tapering and equalizer for 54 × 54 and 134 × 134 UPAs respectively. The elevation and azimuth angles for both figures are 80° and 50°. A short frame was applied for both modulations, that is 16400. The coded rate is 32/45 and 7/9 for 32-APSK and 64-APS respectively. For both figures, the BER rate was improved with both tapering and equalizer at such a higher elevation angle. The variations of the BER have almost matched the broadside elevation angle on both arrays. The scattering plots for EbNo = 10 dB were illustrated in Figures 19 and 20 with and without the tapering and equalizer, respectively. It is clear how the equalizer and tapering are quite effective even for a lower EbNo.

VI. SUMMARIZED CONCLUSION

In this paper, we calculated and presented the frequency response of an array's gain under the assumption of a specific signal bandwidth. We showed the effect of ULA and UPA sizes, as well as four different forms of tapering, on the resulting response. At higher frequencies, the tapering has provided an excellent performance of spreading out the previously narrow differences in the array's response. ZF and MMSE equalisers were implemented to fix the beam squint from the array's gain response. In the majority of the provided examples, the MMSE equalisation performs better than the ZF. Coded and uncoded modulations have been demonstrated among the many instances given. Overall, and especially at greater elevation angles for two array aperture sizes, the analysis shows a significant improvement in BER after applying the tapering and MMSE equalisation. The study also found that with large elevation changes, there will be a decrease in bandwidth and array performance.

REFERENCES

[1] A. Gupta and R. K. Jha, "A survey of 5G network: Architecture and emerging technologies," *IEEE Access*, vol. 3, pp. 1206–1232, 2015.
[2] W. Roh, J.-Y. Seol, J. Park, B. Lee, J. Lee, Y. Kim, J. Cho, K. Cheun, and F. Aryanfar, "Millimeter-wave beamforming as an enabling technology for 5G cellular communications: Theoretical feasibility and prototype results," *IEEE Commun. Mag.*, vol. 52, no. 2, pp. 106–113, Feb. 2014.
[3] T. S. Rappaport, *Wireless Communications: Principles and Practice*, 2nd ed. Upper Saddle River, NJ, USA: Prentice-Hall, 2002.
[4] R. W. Heath Jr., N. González-Prelcic, S. Rangan, W. Roh, and A. M. Sayeed, "An overview of signal processing techniques for millimeter wave MIMO systems," *IEEE J. Sel. Topics Signal Process.*, vol. 10, no. 3, pp. 436–453, Apr. 2016.
[5] V. I. Alekseev, A. N. Anufriev, V. P. Meshchanov, V. V. Semenchuk, and L. V. Shikova, "New structure of ultrawideband fixed phase shifters based on stepped coupled transmission lines with stubs," *J. Commun. Technol. Electron.*, vol. 62, no. 5, pp. 535–541, May 2017.
[6] R. J. Mailloux, *Phased Array Antenna Handbook*, 2nd ed. Norwood, MA, USA: Artech House, 2005.
[7] S. K. Garakoui, E. A. M. Klumperink, B. Nauta, and F. E. van Vliet, "Phased-array antenna beam squinting related to frequency dependency of delay circuits," in *Proc. 41th Eur. Microw. Conf.*, Manchester, U.K., Oct. 2011, pp. 1304–1307.
[8] M. Cai, K. Gao, D. Nie, B. Hochwald, J. N. Laneman, H. Huang, and K. Liu, "Effect of wideband beam squint on codebook design in phased-array wireless systems," in *Proc. IEEE Global Commun. Conf. (GLOBECOM)*, Washington, DC, USA, Dec. 2016, pp. 1–6.
[9] M. Cai, J. N. Laneman, and B. Hochwald, "Beamforming codebook compensation for beam squint with channel capacity constraint," in *Proc. IEEE Int. Symp. Inf. Theory (ISIT)*, Aachen, Germany, Jun. 2017, pp. 76–80.
[10] P. Delos, T. Lead, and B. Broughton, "Phased array antenna patterns—Part 2: Grating lobes and beam squint," *Analog Dialogue*, vol. 54, no. 2, pp. 1–4, 2020.
[11] B. Wang, F. Gao, S. Jin, H. Lin, and G. Y. Li, "Spatial- and frequency-wideband effects in millimeter-wave massive MIMO systems," *IEEE Trans. Signal Process.*, vol. 66, no. 13, pp. 3393–3406, Jul. 2018, doi: 10.1109/TSP.2018.2831628.
[12] B. Wang, F. Gao, S. Jin, H. Lin, G. Y. Li, S. Sun, and T. S. Rappaport, "Spatial-wideband effect in massive MIMO with application in mmWave systems," *IEEE Commun. Mag.*, vol. 56, no. 12, pp. 134–141, Dec. 2018, doi: 10.1109/MCOM.2018.1701051.
[13] B. Wang, M. Jian, F. Gao, G. Y. Li, and I. T. Mar, "Beam squint and channel estimation for wideband mmWave massive MIMO-OFDM systems," pp. 1–30, Mar. 2019, *arXiv:1903.01340v1*.
[14] M. Longbrake, "True time-delay beamsteering for radar," in *Proc. IEEE Nat. Aerosp. Electron. Conf. (NAECON)*, Jul. 2012, pp. 246–249.
[15] H. Huang, K. Liu, R. Wen, Y. Wang, and G. Wang, "Joint channel estimation and beamforming for millimeter wave cellular system," in *Proc. IEEE Global Commun. Conf. (GLOBECOM)*, Dec. 2015, pp. 1–6.
[16] S. Hur, T. Kim, D. J. Love, J. V. Krogmeier, T. A. Thomas, and A. Ghosh, "Millimeter wave beamforming for wireless backhaul and access in small cell networks," *IEEE Trans. Commun.*, vol. 61, no. 10, pp. 4391–4403, Oct. 2013.
[17] M. Cai, J. N. Laneman, and B. Hochwald, "Carrier aggregation for phased-array analog beamforming with beam squint," in *Proc. IEEE Global Commun. Conf. (GLOBECOM)*, Dec. 2017, pp. 1–7, doi: 10.1109/GLOCOM.2017.8254862.
[18] S. Buzzi and C. D'Andrea, "On clustered statistical MIMO millimeter wave channel simulation," 2016, *arXiv:1604.00648*.
[19] I. P. Roberts and S. Vishwanath, "Beamforming cancellation design for millimeter-wave full-duplex," in *Proc. IEEE Global Commun. Conf. (GLOBECOM)*, Dec. 2019, pp. 1–6, doi: 10.1109/GLOBECOM38437.2019.9013116.
[20] J.-S. Jiang and M. A. Ingram, "Spherical-wave model for short-range MIMO," *IEEE Trans. Commun.*, vol. 53, no. 9, pp. 1534–1541, Sep. 2005.

RAED A. ABD-ALHAMEED (Senior Member, IEEE) has been a Professor Research Visitor with Wrexham University, Wales, since 2009, covering the wireless and communications research areas. He is currently a Professor of electromagnetic and radiofrequency engineering with the University of Bradford, U.K. He is also the Leader of radiofrequency, propagation, sensor design, and signal processing with the School of Engineering and Informatics, University of Bradford, where he is also leading the Communications Research Group. He is a Chartered Engineer. He has many years of research experience in the areas of radio frequency, signal processing, propagations, antennas, and electromagnetic computational techniques. He is a Principal Investigator for several funded applications to EPSRCs, Innovate U.K., and the British Council, and the Leader of several successful knowledge transfer programs, such as with Arris (previously known as Pace plc), Yorkshire Water plc, Harvard Engineering plc, IETG Ltd., Seven Technologies Group, Emkay Ltd., and Two World Ltd. He has also been a Co-Investigator in several funded research projects, including 1) Horizan-MSCA-RISE-2024-2028, Marie Skłodowska-Curie, Research and Innovation Staff Exchange (RISE), titled "6G Terahertz Communications for Future Heterogeneous Wireless Network (6G-TERAFIT)"; 2) Horizon Research and Innovation MSCA-RISE-Robust 2022-2027, Marie Skłodowska-Curie, titled "Research and Innovation," titled "FractuRe Orthopaedic Rehabilitation: Ubiquitous eHealth Solution"; 3) Horizon 2020 Research and Innovation Program under Grant H2020-MSCA-RISE-2019-eBORDER-872878; 4) H2020 MARIE Sk[a]odowska-CURIE ACTIONS: Innovative Training Networks Secure Network Coding for Next Generation Mobile Small Cells 5G-US; 5) European Space Agency: Satellite Network of Experts V, Work Item 2.6: Frequency selectivity in phase-only beamformed user terminal direct radiating arrays; 6) Nonlinear and demodulation mechanisms in biological tissue (Department of Health, Mobile Telecommunications & Health Research Program; and 7) Assessment of the Potential Direct Effects of Cellular Phones on the Nervous System (EU: collaboration with six other major research organizations across Europe). He has published over 800 academic journal articles and conference papers; in addition, he has coauthored eight books and several book chapters including seven patents. His research interests include computational methods and optimizations, wireless and mobile communications, sensor design, EMC, beam steering antennas, beamforming, energy-efficient PAs, and RF predistorter design applications. He is a fellow of the Institution of Engineering and Technology and the Higher Education Academy. He was a recipient of the Business Innovation Award for his successful knowledge transfer program with Pace and Datong companies on the design and implementation of MIMO sensor systems and antenna array design for service localizations. He is the chair of several successful workshops on energy-efficient and reconfigurable transceivers: approach toward energy conservation and CO_2 reduction that addresses the biggest challenges for future wireless systems. He has been the General Chair of the IMDC-IST International Conference, since 2020. He has been a Co-Editor of *Electronics* (MDPI), since June 2019. Since 2009, he has been a Guest Editor of *IET Science, Measurement and Technology*.

YIM FUN HU (Senior Member, IEEE) received the B.Sc. degree (Hons.) in mathematical sciences and the Ph.D. degree in information systems engineering, from the University of Bradford, Bradford, U.K., in 1984 and 1987, respectively. She was the Head of the Department of Biomedical and Electronics Engineering, Faculty of Engineering and Informatics, University of Bradford. She is currently a Professor of wireless communication engineering and the Director of the Bradford-Renduchintala Centre for Space AI, Faculty of Engineering and Informatics, University of Bradford. She has published over 150 journal articles and conference papers and coauthored two books and several book chapters. Her research interests include mobile, wireless, and satellite communication networking, including software-defined networking, network function virtualization, mobility management, radio resource management, and network management in 5G networks, applying her research expertise to more than 15 EU and ESA flagship projects in mobile, satellite, aeronautical communications, and fast speed trains as well as many other national, international, and industrial funded projects. She was a fellow of the Institution of Engineering and Technology. She was a recipient of the U.K. Yorkshire Forward Chair in Wireless Communications Engineering.

YASIR AL-YASIR (Member, IEEE) received the B.Sc. and M.Sc. degrees from the University of Basrah, Iraq, in 2012 and 2015, respectively, and the Ph.D. degree from the University of Bradford, U.K., in 2021. In 2014, he joined the Antennas and RF Engineering Research Group, University of Bradford, as a Research Visitor. From 2018 to 2020, he was appointed at the University of Bradford, as a Marie Curie Research Fellow in the H2020-ITN-SECRET Project funded by EU Commission, targeting 5G mobile small cells. He is currently a Staff Member with the Faculty of Engineering and Informatics, University of Bradford. He is also a Research Fellow in the SATNEX-V Project, funded by the European Space Agency. He has authored two books and ten book chapters and published more than 130 journal articles and conference papers on aspects of RF and microwave engineering. His articles have more than 2044 citations with an H-index of 24, as reported by Google Scholar. He was a recipient and a co-recipient of various awards and prizes, such as the Best Paper Award from the IEEE 2nd 5G World Forum and the IEEE 4th 5G Summit Dresden, Germany. He is also a reviewer for various high-ranking journals and publishers, such as IEEE, IET, Wiley, Springer, Elsevier, and MDPI.

NASER OJAROUDI PARCHIN (Senior Member, IEEE) received the Ph.D. degree in electrical engineering from the University of Bradford, U.K. He was a Postdoctoral Research Assistant with the Faculty of Engineering and Informatics, University of Bradford. He was a Research Fellow in the SATNEX V Project, funded by the European Space Agency. From 2014 to 2018, he was with the APMS Section, Aalborg University, Denmark. In 2016, he was a Visiting Researcher with Ankara University, Turkey. From 2018 to 2020, he was a Marie Curie Research Fellow in the H2020-ITN-SECRET Project, funded by the EU Commission, targeting 5G mobile small cells. He is currently an Assistant Professor (Lecturer) with Edinburgh Napier University, U.K. He has over 12 years of research experience in antennas and microwave engineering. His papers have more than 6300 citations with 45 H-index, reported by Google Scholar. His score is higher than 95% of all RG members' scores. He is the author or coauthor of several books/book chapters and more than 300 technical journal articles and conference papers. His research interests include phased arrays, MIMO systems, smartphone antennas, SAR/user-impact, full-duplex diversity, 5G antennas, implementable and biomedical sensors, RFID tag antennas, millimeter-wave and terahertz components, fractal structures, metamaterials/metasurfaces, PCB realization, Fabry resonators, EBG/FSS-inspired radiators, microwave filters, reconfigurable structures, and wireless propagation. He is a member of the Marie Curie Alumni Association (MCAA) and the European Association on Antennas and Propagation (EurAAP). He was a recipient and a co-recipient of various awards and grants for research publications, such as the 2018 Research Development Fund, the 2020/2021 MDPI Travel Award, the Best Paper Award from URSI Symposium 2019, the 5G Summit 2019, the U.K. URSI Festival 2020, IMDC 2021, and ITC-Egypt 2022. He is a Research Grant Reviewer of the Dutch Science Council (NWO). He is also an active reviewer in various high-ranking journals and publishers, such as IEEE TRANSACTIONS, IEEE ACCESS/Letters, IET, Wiley, Springer, Elsevier, and MDPI. He was appointed as a guest editor and a topic board of several MDPI journals. He was included in the World's Top Scientists list, in 2016, 2020, 2021, and 2022.

ATTA ULLAH was born in Mardan, Khyber Pakhtunkhwa, Pakistan. He received the B.Sc. and M.Sc. degrees in electronics engineering from the University of Peshawar, Pakistan, in 1999 and 2002, respectively, the M.Sc. degree in communication engineering from the University of York, U.K., in 2008, and the Ph.D. degree from the Radio Frequency and Sensor Design Research Group, University of Bradford, U.K., in 2022. He was a Research Fellow in the SATNEX V Project, funded by the European Space Agency. His research interests include simulation, design, and implementation of front-end antenna systems for millimeter-wave communications, multi-band/UWB antennas, phased arrays, MIMO systems, smartphone antennas, SAR/user-impact, full-duplex diversity antennas, 5G antennas, implementable/biomedical sensors, RFID tag antennas, millimeter-wave/terahertz components, fractal structures, metamaterials and metasurfaces, Fabry resonators, EBG/FSS-inspired radiators, band-pass/band-stop microwave filters, and reconfigurable structures.